Journal of Materials Chemistry A

Accepted Manuscript

ROYAL SOCIETY OF CHEMISTRY

www.rsc.org/materialsA

Ethynylene-Linked Benzo[1,2-*b*:4,5-*b*′]dithiophene-*alt*-Diketopyrrolopyrrole Alternating Copolymer: Optoelectronic Properties, Film Morphology and Photovoltaic Applications

Hongyu Wang,[a,b,*] Yimin Ding,[a] Yanbang Lai,[a] Zhiwei Sun,[d] Yao Liu,[d] Bin Jiang,[a] Ming Chen,[a] Jian Yao,[a] Feng Liu,[c,*] Thomas P Russell[c, d,*]

ABSTRACT:

Ethynylene-linked benzo[1,2-b:4,5-b′]dithiophene-*alt*-diketopyrrolopyrrole alternating copolymer, **EDPP**, was designed and synthesized to improve the open-circuit voltage of organic solar cells. The influence of the ethynylene on optoelectronic properties, energy levels, crystallinity, film morphology, and photovoltaic performance were investigated. Optical and electrochemical tests showed that introduction of ethynylene into the polymer backbone resulted in a larger bandgap, deeper HOMO energy level, and enhanced crystallinity due to the planar conformation and electron-withdrawing properties. Grazing incidence wide-angle X-ray scattering (GIWAXS) showed that the pure **EDPP** film preferentially adopted a face-on orientation with a π-π stacking distance of 3.65 Å. After thermal annealing the

[a] Department of Chemistry, Shanghai University, Shanghai 200444, China. E-mail: wanghy@shu.edu.cn

[b] State Key Laboratory of Molecular Engineering of Polymers (Fudan University), Shanghai 200433, China

[c] Materials Sciences Division, Lawrence Berkeley National Laboratory, Berkeley, CA, 94720, USA. Email: iamfengliu@gmail.com

[d] Department of Polymer Science and Engineering, University of Massachusetts, Amherst, MA, 01003, USA. Email: Russell@mail.pse.umass.edu

face-on and edge-on orientations coexisted and the overall degree of crystallinity increased. Blending with $PC_{71}BM$ did not disrupt the crystallinity of the **EDPP**. Resonant soft X-ray scattering (RSoXS) showed that the **EDPP**:$PC_{71}BM$ blend films contained large domains, a few hundred nanometers in size. As a result, **EDPP**:$PC_{71}BM$ photovoltaic devices exhibited a high open-circuit voltage of 0.88 V, but a low short-circuit current, with a moderate power conversion efficiency of 1.98%.

Introduction

Bulk heterojunction (BHJ) organic photovoltaics (OPVs) have drawn attention as a promising technology for renewable energy in recent years due to the advantages of solution processability, low cost, light-weight, and flexibility. To get a BHJ device to function efficiently, usually a donor material, which plays a major role in light absorption, exciton generation and hole-conduction; and an acceptor material, which creates electron pathways, are required.[1,2] The intrinsic properties of commercially available fullerenes show high electron affinities and mobilities and, consequently, are widely as electron acceptors in BHJ devices.[3,4] From the perspective of electron donor materials, low band-gap conjugated polymers consisting of alternating electron-rich (donor, D) and electron-deficient (acceptor, A) units in the conjugated backbone have proven to be an effective strategy in achieving high performance OPVs, since their absorption can be extended to longer wavelengths via internal charge transfer (ICT) and their electronic properties can be easily tuned by varying the donor and acceptor

units.[5,6] For most reported D-A copolymers, the donor and acceptor units are connected by carbon-carbon single bonds in the polymer main chain, due, in part, to the availability of the efficient protocols for metal-catalyzed polycondensation of organometallic aryl monomers and aryl halides, like the Suzuki,[7,8] Stille,[9,10] Nigishi,[11] and Kumada cross-coupling reactions,[12] etc. The linkage of carbon-carbon single bond can extend the conjugation length but may also produce a fairly large twist angle between repeat units along the backbone due to steric hindrance between the neighboring carbon-carbon bonds.[13,14] For example, one of the most well-studied polymer donor, thieno[3,4-*b*]thiophene-*alt*-benzodithiophene copolymer (PTB7), prepared by Palladium-catalyzed Stille cross-coupling reaction, was found to be nonplanar with an average inter-ring torsional angle of ~25° by first-principles calculations.[15,16] Such a steric twisting disturbs the formation of a more extended conjugation length and hinders efficient intermolecular stacking and solid-state packing. Insertion of unsaturated linkages (e.g., ethynylene and ethylene) between the donor and acceptor units has been recognized as a promising strategy to reduce steric hindrance and enhance coplanarity along the polymer backbone, which is beneficial for high charge carrier mobilities.[17-21]

Poly(arylacetylenes) have attracted a significant amount of interest from the organic electronics community.[22,23] Much of the research on these materials has focused on applications of their high fluorescent quantum efficiency characteristics, including metal ions sensing,[24,25] organic light-emitting diodes (OLEDs),[26] and bioimaging applications.[27] Furthermore, poly(arylacetylenes) possess unique

properties for OPV applications. Due to the electron-withdrawing nature of the ethynylene group, poly(arylacetylenes) usually have lower the highest occupied molecular orbitals (HOMO) over their analogues linked by carbon-carbon single bond, leading to higher open-circuit voltage (V_{oc}) in organic solar cells.[17,28] Hence, ethynylene-containing materials have been used in small molecules,[29-32] polymers,[33-36] and metallopolyyne photovoltaic materials.[37-39] Janssen *et al.* reported that incorporating ethynylene units into the poly(3-hexylthiophene) (P3HT) backbone could result in 0.3 eV lowering of the HOMO level, thus achieving a high V_{oc} of 1.01 V, giving a significant improvement (0.4 V) of V_{oc} with respect to P3HT:PCBM solar cells.[28] Troshin, Facchetti, and Wong *et al.* reported the phenylene-vinylene-phenyleneethynylene copolymers,[40] branched arylacetylenic small molecules,[41] and Pt-acetylide-based oligomers and polymers,[37,38] respectively, achieving the PCE of 3~4.93%. Recently, Braunecker *et al.* made a comparative study between a series of ethynylene-linked D-A conjugated polymers and their fully cyclic analogues. The authors found that the introduction of ethynylene linkages into the D-A systems universally resulted in planar conformations, significant blue-shift of absorbance, and a deeper HOMO value.[17] So far, the ethynylene-containing D-A conjugated polymers have been only marginally explored, and their applications in OPV devices only achieved modest PCEs (generally < 4%).[20] The effect of ethynylene linkages on the BHJ morphology remains poorly understood.

In 2009, Yang and coworkers firstly reported the alternating copolymer Poly(BDT-DPP) (Scheme 1) based on 4,8-dioctyloxy-substituted

benzo[1,2-*b*:4,5-*b*′]dithiophene (BDT) and 2-ethylhexyl-substituted diketopyrrolopyrrole (DPP).[42] Although Poly(BDT-DPP) exhibited a low band-gap of 1.31 eV and broad light absorption range of 300~900 nm, the BHJ devices showed only moderate PCE of 2.53% with an V_{OC} of 0.68 V, due to a relatively high-lying HOMO level of 5.16 eV. Thereafter, intensive efforts have been made to improve photovoltaic performance of copolymers based on BDT and DPP, in which incorporating alkylthienyl or alkylphenyl moieties onto the BDT unit and replacement of the neighboring thiophene units on the DPP core with either furan or selenophene rings have been developed, leading to further improvement of the PCE over 8%, which is among the highest PCE values for the single-cell device.[43-45] It is worthy to note that Poly(BDT-DPP) copolymers usually display high-lying HOMO level, and, thus, yield relatively modest V_{OC} values, which is a limiting factor for high efficiency OPVs. It is well known that D-A conjugated polymers composed of "weak donor" unit are beneficial for a low-lying HOMO level.[47] One of the most widely used methods to gain the low-lying HOMO level is addition of pendant electron-withdrawing substituents such as fluorine, cyano or carboxy groups directly to the donor unit. Yu *et al.* successively introduced fluorine atoms into the thienothiophene (TT) and BDT units of the PTB, and the HOMO levels of the resulting polymers were lowered by ~0.54 eV.[16] Jo *et al.* reported that removing the strong electron-donating alkoxy-substituents from 4,8-positions of BDT could possess a considerably lower HOMO (-5.46 eV) than those dialkoxy-functionalized Poly(BDT-DPP) (-5.29 eV), and thus a higher V_{OC} value of 0.82 V was achieved.[48]

Here, we introduce the electron-withdrawing ethynylene units into the polymer backbone to reduce their HOMO energy levels. An ethynylene-linked BDT-*alt*-DPP copolymer **EDPP** was synthesized by Sonogashira cross-coupling reaction (Scheme 1). And the polymer **PBDTDPP** bearing a similar chemical structure but without ethynylene-bridge was also synthesized to compare with **EDPP**, thereby allowing us to focus solely on the impact of ethynylene units. As expected, **EDPP** indeed showed a deep HOMO of -5.68 eV, and thus a high V_{oc} of 0.88 V was achieved when blending with $PC_{71}BM$. Optical and electrochemical tests showed that introduction of ethynylene into the polymer backbone resulted in a larger band-gap and deeper HOMO energy level. To better understand the influence of ethynylene on the photovoltaic performance, bulk heterojunction blended thin film morphology was systematically characterized by grazing incidence wide-angle X-ray scattering (GIWAXS), atom force microscopy (AFM), and resonant soft X-ray scattering (RSoXS).

Experimental

Materials

All chemicals and reagents were used as received from commercial sources. Anhydrous tetrahydrofuran (THF) and toulene were distilled from sodium/benzophenone ketyl prior to use. 2,6-Bis(trimethyltin)-4,8-di(2-octyldodecyloxy)benzo[1,2-*b*:4,5-*b'*]dithiophene **5** was purchased from SunaTech Inc. (http://www.sunatech.com.cn). The monomers **1** and **4**

were synthesized according to the literature.[42]

General measurement and characterization

The NMR spectra were collected on a Varian Mercury Plus 500 spectrometer with tetramethylsilane as the internal standard. UV-Vis spectra were recorded on a Shimadzu 3150 PC spectrophotometer. TGA measurements were performed on a Netzsch TG209 apparatus. DSC measurements were performed on a PerkinElmer DSC 7 instrument with approximate 5 mg samples at a heating rate of 10 °C min^{-1} under N_2. GPC analysis of the copolymers was performed on a Shimadzu 10A series with THF as the eluent and polystyrene as the standard for calibration. FTIR spectra were recorded on a JASCO FT/IR-470 plus Fourier transform infrared spectrometer and measured as KBr pellets. Cyclic voltammetry (CV) was performed at a scanning rate of 50 mV s^{-1} on an AUTOLAB.PGSTAT30 potentiostat/galvanostatsystem (Ecochemie, Netherlands), which was equipped with a three-electrode cell. The sample was cast onto a glass carbon disk as the working electrode and Pt wire was used as the counter electrode. An Ag/Ag^+ was used as the reference electrode. Tetrabutylammoniumhexafluorophosphate (n-Bu_4NPF_6, 0.1 mol L^{-1}) was used as a supporting electrolyte. Atom force microscopy was performed on a Digital Instruments Dimension 3100, operating in tapping mode. Grazing incidence wide-angle X-ray scattering (GIWAXS) measurements were performed on Beamline 7.3.3 at the Advanced Light Source at the Lawrence Berkeley National Laboratory. An X-ray beam impinged onto the sample at a grazing angle above the critical angle of the polymer film (α_c = 0.16) but below the critical angle of the silicon substrate (α_c

= 0.24). The wavelength of X-rays used was 1.240 Å, and the scattered intensity was detected by using PILATUS 1M detector. RSoXS was performed at beamline 11.0.1.2 Lawrence Berkeley National Lab. Thin films was flowed and transferred onto Si_3N_4 substrate and experiment was done in transmission mode.

Fabrication and characterization of photovoltaic cells

The indium tin oxide (ITO)-coated glass substrates (20 ± 5 ohms/sq) were bought from Thin Film Devices Inc., and were cleaned through ultrasonic treatment in detergent, DI water, acetone, and isopropyl alcohol and then dried in an oven overnight. PEDOT: PSS (Baytron P VP A1 4083) (~ 35 nm) was spin-coated on the ultraviolet ozone-treated ITO substrates. After annealing at 150 ^{o}C for 30 min in air, the substrates were transferred to the glove box. Polymer/$PC_{71}BM$ dichlorobenzene (DCB) solution (10 mg/mL of polymer concentration) was spin-coated on top of the PEDOT: PSS layer at 3000 rpm. The thickness of film was ~ 80-100 nm (KLA-TENCOR Alpha-Step IQ Surface Profiler). Finally, ~5 nm of poly [(9,9-bis(3′-(*N*,*N*-dimethylamino)propyl)-2,7-fluorene) -alt-2,7-(9,9- dioctylfluorene)] (PFN) or 1 nm LiF and then 100 nm thick Al cathode was deposited (area 6.5 mm^2) on the active layer under high vacuum (2×10^{-4} Pa) using a thermal evaporator. All current-voltage (*J-V*) characteristics of the devices were measured under simulated AM1.5G irradiation (100 mW cm^{-2}) using a Xe lamp-based Newport 91160 300-W solar simulator. A Xe lamp equipped with an AM1.5G filter was used as the white light source. The light intensity was adjusted with an NREL-calibrated Si solar cell with a KG-5 filter.

2,6-Bis(trimethylsilylethynyl)-4,8-bis(2-octyldodecyloxy)benzo[1,2-*b*:4,5-*b'*]dithiophene (2).

Compound **1** (941.1 mg, 1 mmol), ethynyl trimethlsilane (245.6 mg, 2.5 mmol), tetrakis(triphenylphosphine) palladium (4 mg), and cuprous iodide (2 mg) were added to a mixture of anhydrous THF (5 mL) and diisopropylamine (5 mL). The mixture was vigorously stirred at 60 ^{o}C for 24 h under nitrogen. After cooling to room temperature and removal of the solvent under reduced pressure, the crude product was purified by column chromatography using a mixture of dichloromethane and hexane (v/v = 1/20) as eluent to afford pale yellow solid (yield: 70%, 683 mg). ^{1}H NMR (500 MHz, $CDCl_3$): δ 7.55 (s, 2H), 4.15 (d, J = 5.4 Hz, 4H), 1.87-1.83 (m, 2H), 1.61-1.20 (m, 66H), 0.91-0.88 (m, 12H), 0.29 (s, 18H).

2,6-Diethynyl-4,8-bis(2-octyldodecyloxy)benzo[1,2-*b*:4,5-*b'*]dithiophene (3).

Compound **2** (722.1 mg, 0.74 mmol), KOH (82.8 mg, 1.48 mmol) were added to a mixture of MeOH (3 mL) and THF (6 mL). The reaction mixture was stirred for 6 h at room temperature, then quenched with NH_4Cl (aq.) and extracted with dichloromethane. The organic fraction was washed with water and dried over sodium sulfate. The crude product was purified by column chromatography using a mixture of dichloromethane and hexane (v/v = 1/9) as eluent to afford pale yellow solid (yield: 90%, 553.7 mg). ^{1}H NMR (500 MHz, $CDCl_3$): δ 7.63 (s, 2H), 4.14 (d, J = 5.39 Hz, 4H), 3.49 (s, 2H), 1.87-1.83 (m, 2H), 1.61-1.20 (m, 66H), 0.91-0.88 (m, 12H). ^{13}C NMR (500 MHz, $CDCl_3$): δ 144.14, 131.56, 129.92, 126.56, 121.89, 114.10, 83.32, 39.21, 32.00, 31.98, 31.27, 30.10, 29.77, 29.73, 29.69, 29.44, 29.43, 27.00, 22.75,

14.17.

Polymerization of EDPP.

Monomer **3** (158.6 mg, 0.19 mmol), monomer **4** (194.5 mg, 0.19 mmol), tetrakis(triphenylphosphine) palladium (8 mg), and cuprous iodide (4 mg) were added to a mixture of THF (5 mL) and diisopropylamine (5 mL). The mixture was vigorously stirred at 75 ^{o}C for 48 h under nitrogen. After cooling to room temperature, the reaction mixture was poured into a large volume of methanol. The precipitation was collected and further purified by Soxhlet extraction with methanol, acetone, hexane and chloroform successively. The polymer was recovered as solid from the chloroform fraction by rotary evaporation. After drying under vacuum overnight, a dark red solid was obtained with a yield of 63%. ^{1}H NMR (500 MHz, $CDCl_3$): δ 8.95 (br, 2H), 7.8-7.2 (br, 4H), 4.20-4.05 (br, 8H), 2.0-0.87 (br, 160H). M_n = 46.3 kg/mol; polydispersity = 2.55.

Polymerization of PBDTDPP.

Monomer **5** (221.79 mg, 0.2 mmol), **4** (203.84 mg, 0.2 mmol), and tetrakis(triphenylphosphine) palladium (15 mg) were put into a round-bottom flask under the protection of nitrogen, then 7 mL of degassed toluene was added. The mixture was vigorously stirred at 100 ^{o}C for 48 h. After cooling to room temperature, the reaction mixture was poured into a large volume of methanol. The precipitation was collected and further purified by Soxhlet extraction with methanol, acetone and finally chloroform successively. The polymer was recovered as solid from the chloroform fraction by rotary evaporation. After drying under vacuum overnight, a

dark red solid was obtained with a yield of 70%. ^{1}H NMR (500 MHz, $CDCl_3$): δ 9.22 (br, 2H), 7.66-7.13 (br, 4H), 4.23-4.11 (br, 8H), 2.0-0.87 (br, 160H). M_n = 10.2 kg/mol; polydispersity = 2.11.

Results and Discussion

Synthesis and characterization

The synthetic route and structure of **EDPP** and **PBDTDPP** are shown in Scheme 1. To ensure the solubility of the polymer, 2-octyldodecyl chains were attached to nitrogen of the lactam in DPP unit and the oxygen atoms of 4,8-positions of BDT unit, respectively. **PBDTDPP** was synthesized by Stille coupling reaction following the method reported in the literature.[42] **EDPP** was synthesized vis a Sonogashira coupling reaction using $Pd(PPh_3)_4$ and CuI as catalysts in a mixed solvents of toluene and diisopropylamine at 75 ^{o}C for 48 h. Both polymers were highly soluble in common organic solvents such as THF, chloroform, chlorobenzene (CB) and DCB without gel formation. The ^{1}H NMR spectrum of **EDPP** displayed broad resonance peaks of the polymeric characters. The peak at about 8.95 ppm could be assigned to the DPP thienyl protons, which appeared at a lower field than the DPP monomer **4** (8.64 ppm). The other aromatic protons of **EDPP** showed broad resonance peaks ranging from 7.8 to 7.2 ppm. The signals of the methylene adjacent to nitrogen of the lactam group in DPP units and oxygen of BDT units appeared around 4.2 and 4.0 ppm, respectively (Fig. S1). From FTIR results, the presence of absorption peaks around 2180 cm^{-1} assignable to ethynylene moiety and the absence of the terminal ethynyl peaks

(stretching vibration around 3300 and 2100 cm^{-1}) also supported the formation of ethynylene-linked polymer (Fig. S2).[49] The number-average molecular weights for **EDPP** and **BDTDPP** were 46.3 and 10.2 kg/mol with a polydispersity of 2.55 and 2.11, respectively, as determined by gel permeation chromatography (GPC) with THF as an eluent against polystyrene standards (Fig. S3). The thermal properties of **EDPP** was investigated by thermogravimetric analysis (TGA) and differential scanning calorimetry (DSC) at a heating rate of 10 ^{o}C min^{-1} under nitrogen atmosphere (Fig. S4-5). The onset of thermal degradation temperature (5% weight loss) of **EDPP** was recorded at about 340 ^{o}C, showing excellent thermal stability for solar cell applications. However, no apparent thermal transitions were observed from DSC characterization while heating from 30 to 250 ^{o}C. It should be noted that in later X-ray investigations that structure order was seen for **EDPP**, which contradicts DSC observations. The reason for this discrepancy can be two folds: (1) the low crystallinity nature in bulk and slow crystallization kinetics makes **EDPP** thermal behavior can be hardly observed in DSC scan; (2) X-ray measurement was done in thin film geometry, which might lead to better structure.

Optical absorption and electrochemical properties

Fig. 1 showed the UV-Vis absorption spectra of **EDPP** and **PBDTDPP** recorded in both chloroform solution and thin films. And the corresponding data were listed in Table 1. In dilute solution, **EDPP** exhibited broad absorption in the range of 300~800 nm with two distinct energy bands. The absorption band in around 300~500 nm could be assigned to π-π^* transition of the conjugated main chain. And the second broad

absorption band from 500~800 nm in the long wavelength region exhibited two peaks at 645 and 703 nm. The first peak originated from the ICT between BDT donor and DPP acceptor, and the second peak originated from polymer chain stacking (J-type). The absorption spectrum of **EDPP** in solution was similar to that of the thin film, and the maximum absorption peak was slightly red-shifted from 703 nm to 707 nm. These results indicated that **EDPP** polymer chain formed aggregated structure in chloroform solutions, which most probably came from the flattened backbone structure induced by ethylnylene linkage.[18,19,50,51] This could be verified by the absorption measured at an elevated temperature of 50 ^{o}C, in which the absorption peak of the aggregate was blue-shifted from 703 nm (25 ^{o}C) to 694 nm (50 ^{o}C) and the absorption intensity was reduced significantly. The 707 nm absorption peak in the solid film became broader and showed a much higher intensity than that measured in solution, indicating better ordering of chains during solidification. A ~15 nm red-shift in the absorption onset point was seen from solution to thin film absorption, showing a band gap narrowing induced by structure ordering. **PBDTDPP** exhibited the similar absorption characteristics as compared to literature analogue of Poly(BDT-DPP) with different alkyl chains.[42] However, the introduction of ethynylene units into the main chain resulted in a blue-shift in the absorbance spectra in both solution and the solid state compared to **PBDTDPP**,[42,52] which implied that the ICT between BDT and DPP moieties was not as efficient as directly linking them together.[17] The maximum extinction coefficient of **EDPP** was 6.19×10^4 M^{-1} cm^{-1}, slightly higher than that of **PBDTDPP** (5.22×10^4 M^{-1} cm^{-1}). This slight increase in absorption for **EDPP** could

be attributed to the introduction of the ethynylene chromophore into the backbone. The optical band gaps of **EDPP** and **PBDTDPP** based on optical absorption edges of the film spectra were 1.55 and 1.31 eV, respectively.

The electrochemical characteristics of **EDPP** were studied by cyclic voltammetry (CV) using 0.1 M n-Bu_4NPF_6 as the electrolyte at a scan rate of 50 mV s^{-1}. The redox potentials of the polymers were referenced to the ferrocene/ferroceenium (Fc/Fc^+) redox couple (absolute energy level of -4.8 eV relative to a vacuum).[53] As shown in Fig. 2, **EDPP** exhibits one reversible reduction wave and one irreversible oxidation wave. The oxidation and reduction onsets appeared at 0.85 and -1.2 V, respectively, corresponding to HOMO and LUMO energy levels of -5.68 and -3.63 eV. For **PBDTDPP**, the oxidation and reduction onsets appeared at 0.60 and -1.22 V, respectively, corresponding to HOMO and LUMO energy levels of -5.43 and -3.61 eV. The introduction of ethynylene units into polymer backbone significantly reduce the HOMO level by ~0.25 eV with respect to the fully heterocyclic analogue **PBDTDPP**,[42,54] which is consistent with literature results.[28] Hence, a higher V_{oc} in **EDPP**-based OPVs could be expected due to its deeper HOMO level. The calculated electrochemical bandgap of **EDPP** was 2.03 eV, which was about 0.5 eV larger than the optically determined one (1.55 eV). Similar differences had been seen in the literatures, which could be attributed to the exciton binding energy of conjugated polymers, in the range of ~ 0.4-1.0 eV.[18,55]

Photovoltaic properties

The photovoltaic characteristics were investigated with the device architecture of

ITO/PEDOT:PSS/polymer:$PC_{71}BM$/PFN/Al. Due to the formation of a surface dipole at interface between the photoactive layer and metal electrode, thus suppressing the interfacial recombination, conjugated polyelectrolyte PFN was prepared on the top of the photoactive layer as cathode buffer.[56] BHJ devices based on **EDPP**:$PC_{71}BM$ blends were fabricated and tested under the illumination of AM 1.5G, 100 mW cm^{-2}. The active layers were optimized by varying the **EDPP**:$PC_{71}BM$ blends under different weight ratios (2 : 1, 1.5 : 1, 1 : 1, 1 : 2). Fig. 3 shows the current density-voltage (*J*–*V*) curves, and the photovoltaic data of the devices are summarized in Table 2. The J_{sc} exhibited a strong dependence on the **EDPP**:$PC_{71}BM$ weight ratios. Decreasing the **EDPP** content in the active layer from 2 : 1 to 1: 1, J_{sc} increased from 2.84 to 5.67 mA cm^{-2}. Then J_{sc} started to drop when further decreasing the **EDPP** content. Fill factor (FF) showed similar trend, but the maximum value (45%) appeared at the weight ratio of 1.5 : 1. In general, the fill factors for these devices were low. The possible reason for the low fill factor in BHJ devices most probably came from strong recombination, which strongly limited device performance. Different from J_{sc} and FF, V_{oc} almost kept constant (0.84~0.88 V).[57] Finally, with the optimized weight ratio of **EDPP**:$PC_{71}BM$ at 1: 1, a best but moderate PCE of 1.98% was achieved, with a J_{sc} of 5.67 mA cm^{-2}, a V_{oc} of 0.88 V, and a FF of 39%. The external quantum efficiency (EQE) curve of the optimized device was shown in Fig. 4. The EQE curve of the device covered a broad range from 300 to 800 nm, showing contributions from both **EDPP** and $PC_{71}BM$. However, the EQE value was not high, and that was the reason for its low current. Photovoltaic device of

PBDTDPP:$PC_{71}BM$ blend was also fabricated at 1:1 weight ratio to compare with **EDPP** polymer OPV performance. **PBDTDPP**:$PC_{71}BM$ device showed a reasonable V_{oc} of 0.66 V, which was consistent with the literature analogue of Poly(BDT-DPP).[42,45] However, the low J_{sc} of 1.48 mA cm^{-2} and FF of 39% limited the device performance with a poor PCE value of 0.37%, which could be partially attributed to the low molecular weight of **PBDTDPP**. Notably, **EDPP** exhibited relatively high V_{oc}, due to its low-lying HOMO level, which was about 0.22 eV higher than that of **PBDTDPP** based device. Although the V_{oc} was significantly improved by introduction of ethynylene group into the backbone, relatively low J_{sc} and FF limited the overall performance of the **EDPP**:$PC_{71}BM$ devices. Similar phenomena have been reported by Janssen *et al*.,[28] where incorporating ethynylene units into the poly(3-hexylthiophene) (P3HT) backbone could result in a significant improvement (0.4 V) of V_{oc} compared to P3HT:PCBM devices.

Grazing incidence wide-angle X-ray scattering (GIWAXS)

The crystalline properties, such as the chain registration and crystal orientation of pure polymer and polymer:$PC_{71}BM$ blends are investigated using GIWAXS. Experiments were carried out in helium chamber to reduce air scattering. The 2D diffraction profiles are shown in Fig. 5 and out-of-plane and in-plane line-cut profiles are shown in Fig. 6. The corresponding data are summarized in Table 3. In the pristine film, **EDPP** showed semicrystalline properties where a broad diffraction halo ring existed at q = 1.4 $Å^{-1}$ was attributed to scattering from amorphous regions within the **EDPP** film. A strong out-of-plan diffraction peak at q_z = 1.72 $Å^{-1}$ could be seen,

which corresponds to a distance of 3.65 Å and is attributed to π-π stacking. This π-π stacking distance is obviously shorter than that of **PBDTDPP** (3.9 Å),[58] which is due to the better coplanarity and rigidity of ethynylene group, thus facilitating closer stacking. Also, a sharp and intense diffraction peak at q_{xy} = 0.28 $Å^{-1}$ in the in-plane direction was observed, which comes from (1 0 0) lamellar stacking of alkyl chains with a d-spacing of 22.4 Å. These diffraction patterns show that **EDPP** preferentially adopt a highly ordered face-on orientation with respect to the substrate, which is obviously different from the patterns in **PBDTDPP** film in that polymer chains assumed random orientations without a significant preference for edge-on or face-on orientations.[58] When thermally annealed at 200 ^{o}C for 30 min, a strong diffraction peak at about q_z = 0.3 $Å^{-1}$ in the out-of-plane direction is seen, suggesting formation of the edge-on orientation. At the same time, (1 0 0) peak in the in-plane direction and the (0 1 0) peak in the out-of-plane still showed high intensity. Therefore, thermal annealing induces the growth of edge-on crystallites from amorphous materials and the face-on orientation is sustained. The Scherrer equation was used to estimate the crystal correlation length (CCL) from the full width at half maxima (FWHM) of (1 0 0) lamellar stacking. The CCL of the annealed film was increased to 23.5 nm, which was about 4.2 nm larger than that of the as-cast film (19.3 nm). The area of both (1 0 0) and (0 1 0) peaks showed enhancement upon thermal annealing, indicating a better order for annealed thin film. In blends, the amorphous halo of the polymers overlaps with the $PC_{71}BM$ scattering (~1.35 $Å^{-1}$), making it difficult to assess the structure information of $PC_{71}BM$. **EDPP** polymer in blends primarily assumes a face-on

orientation, as indicated from strong (0 1 0) reflection in the out-of-plane direction. The characteristic (1 0 0) and (0 1 0) diffraction peaks remained almost at the same positions relative to that for the pure polymer film. This indicates that the lamellar and π-π stacking distances of the polymer chains were not significantly influenced in the presence of $PC_{71}BM$, and no $PC_{71}BM$ molecule was intercalated between the polymer chains.[59] Consistent with this, the FWHM of (1 0 0) reflection remained almost the same as in the as-cast film, indicating the same CCL in the blend films.

BHJ Morphology

The morphology of the active layer is one of the key factors determining the photovoltaic performance. The different performance of **EDPP**:$PC_{71}BM$ blend films was further analyzed by atomic force microscopy (AFM) and resonant soft X-ray scattering (RSoXS). The surface morphologies of **EDPP**:$PC_{71}BM$ blend films with different weight ratios were characterized using tapping-mode AFM (Fig. 7). Note that these blend films were prepared according to the device procedure. The surfaces of all the films are fairly smooth and uniform. Varying the blend ratio of **EDPP**:$PC_{71}BM$, the root-means-square (RMS) roughness of the blend films firstly decreases slightly from 1.69 (2 : 1) to 1.22 nm (1 : 1), then increasing to 2.37 nm (1 : 2). Because phase contrast is related to the difference in adhesive and mechanical properties of individual materials, which indicates that the dark and bright regions correspond to different components.[60] Large domain size of several hundreds of nanometers and discontinuous phase separation can be clearly observed in Fig. 6 a′ and b′ when blending with 2 : 1 and 1.5 : 1 weight ratios, which is not beneficial for

excitons dissociation and charge transport, thus resulting in low J_{sc} and FF. When decreasing the **EDPP** content to 1 : 1, the domains appear to become better defined and smoother, but still larger than the tens of nanometers. Further decreasing the weight ratio to 1:2, both height image and phase image changed strongly, indicating a high PCBM load significantly changes the phase separation and physical properties of the film.

AFM allow us to probe the morphology at the top surface of the film; however, it provides little information about the bulk morphology. Resonant soft X-ray scattering (RSoXS) was utilized to investigate the bulk morphology of the blend films. In RSoXS experiment, the beam energy was tuned to 284.2 eV, which is at the carbon K-edge to enhance the contrast of the PCBM and polymer. Fig. 8 shows the RSoXS profiles of **EDPP**:$PC_{71}BM$ blend films. The 2 : 1 **EDPP**:$PC_{71}BM$ blend film showed dual scattering peaks: a scattering peak at ~ 0.0014 $Å^{-1}$ and a shoulder at ~ 0.006 $Å^{-1}$, corresponding to center-to-center spacing of 450 and 100 nm, respectively. Thus a hierarchical morphology existed in this thin film. It was expected that the large size of phase separation was the inter spacing of PCBM rich domains, and the 100 nm phase separation was polymer crystal inter spacing. When the **EDPP** content decreased to 1.5 : 1 and 1 : 1, the intensity of scattering peak at ~ 0.0014 $Å^{-1}$ was gradually reduced, while the intensity of the shoulder (~ 0.006 $Å^{-1}$) became increasingly intense and the position slightly shifted to low q value. In the 1 : 1 **EDPP**:$PC_{71}BM$ blend film, the dominant domain spacing was about 140 nm (0.0044 $Å^{-1}$). The increase of PCBM content leads to permissive distribution of PCBM inside BHJ thin film and no isolated

PCBM rich domain can be discerned. The inter-crystal distance was also increased due to PCBM swelling of the entire film. Further reduction of **EDPP** content to 1 : 2, the scattering peak became more intense, and exhibited broad distribution towards low q region. This was because overloading of PCBM led to aggregation of isolated PCBM domains, which gave rise to a new spacing in scattering. The inter-crystal spacing should close to or slightly larger than 1 : 1 case. A reduction in performance was expected due to the reduction in absorption since fewer polymer was used. However the existence of a similar inter-crystal spacing would still generate a fair amount of current, thus the performance drop would not be disastrous. These results were consistent with the photovoltaic devices characterization, where 1 : 1 **EDPP**:$PC_{71}BM$ blend films achieved the optimized photovoltaic performance. It should be noted that adding 1,8-diiodooctane (DIO) additive does not strongly boost the performance of the devices (results shown in supporting information), since no strong PCBM aggregation was seem in the BHJ thin film. In fact addition of additive led to more PCBM aggregation and slightly enlarged the size of phase separation, thus a drop in performance was recorded. It should also be noted that the observed phase separation was mainly due to the strong polymer crystallization. We observed a ~20 nm of (1 0 0) crystal size. Polymer crystals assume a face-on orientation, and the (1 0 0) direction was in-plane. The ~100 nm phase separation best described the inter-crystal spacing by taking account of amorphous polymers and PCBM. Thus, such a large crystal size was not ideal to keep the length scale of phase-separated domains on the tens of nanometer level, explaining the moderate performance of this

family of materials.

Conclusions

Ethynylene-linked D-A copolymer **EDPP** based on BDT and DPP units was synthesized by Sonogashira coupling reaction. Compared to the fully heterocyclic analogue **PBDTDPP**, introduction of ethynylene units into polymer backbone resulted in the blue-shift of the maximum absorption. Cyclic voltammetry measurements revealed that **EDPP** had a low-lying HOMO level of -5.68 eV, which was about ~0.25 eV lower than that of **PBDTDPP**. **EDPP**:$PC_{71}BM$ devices gave a significant (0.22 V) improvement of V_{OC} with respect to **PBDTDPP**:PCBM solar cells. With the optimized weight ratio of **EDPP**:$PC_{71}BM$ at 1: 1, a best but moderate PCE of 1.98% was achieved, with J_{sc} of 5.67 mA cm^{-2}, V_{oc} of 0.88 V, and FF of 39%. GIWAXD revealed that **EDPP** preferentially adopt a face-on orientation with respect to the substrate. RSoXS suggested that the **EDPP**:$PC_{71}BM$ blends formed the large phase separation domains around 100 nm, which is the major reason for the low J_{sc} . This study demonstrates that introduction of ethynylene units into the polymer backbone is an effective method to improve the V_{oc} of photon active materials. However, to get an overall enhance performance in OPV device need to focus more on size of phase separation. Too large crystal size will prohibit a refined phase separation and thus no optimized J_{sc} can be obtained. Thus a more comprehensive material design including modifying structures to directly tuning morphology is a must in developing better performance materials.

Acknowledgments

This work was financially supported by the National Natural Science Foundation of China (Grant Nos. 61204020). FL and TPR were supported by Polymer-Based Materials for Harvesting Solar Energy (PHaSE), an Energy Frontier Research Center funded by the U.S. Department of Energy, Office of Basic Energy Sciences under award number DE-SC0001087. Portions of this research were carried out at beamline 7.3.3 and 11.0.1.2 at the Advanced Light Source, and Molecular Foundry, Lawrence Berkeley National Laboratory, which was supported by the DOE, Office of Science, and Office of Basic Energy Sciences.

Notes and references

1 G. Yu, J. Gao, J. C. Hummelen, F. Wudl, A. J. Heeger, *Science*, **1995**, 270, 1789-1791.

2 F. Liu, Y. Gu, J. W. Jung, W. H. Jo, T. P. Russell, *J. Polym. Sci. Poly. Phys.*, **2012**, 50, 1018-1044.

3 B. C. Thompson, J. M. J. Fréchet, *Angew. Chem. Int. Ed.*, **2008**, 47, 58-77.

4 L. Y. Lin, C. W. Lu, W. Ch. Huang, Y. H. Chen, H. W. Lin, K. T. Wong, *Org. Lett.*, **2011**, 13, 4962-4965.

5 Y. J. Cheng, S. H. Yang, C. S. Hsu, *Chem. Rev.*, **2009**, 109, 5868-5923.

6 H. Y. Wang, J. Gao, W. Q. Tong, Q. Qian, K. H. Lin, F. Liu, *Polym. Chem.*, **2012**, 3, 2794-2800.

7 N. Blouin, A. Michaud, M. Leclerc, *Adv. Mater.*, **2007**, 19, 2295-2300.

8 O. Inganäs, F. Zhang, M. R. Andersson, *Acc. Chem. Res.*, **2009**, 42, 1731-1739.

9 H. Y. Wang, J. Gao, L. J. Gu, J. H. Wan, W. Wei, F. Liu, *J. Mater. Chem. A*, **2013**, 1, 5875-5885.

10 C. Cabanetos, A. E. Labban, J. A. Bartelt, J. D. Douglas, W. R. Mateker, J. M. J. Fréchet, M. D. McGehee, P. M. Beaujuge, *J. Am. Chem. Soc.*, **2013**, 135, 4656-4659.

11 T. A. Chen, X. M. Wu, R. D. Rieke, *J. Am. Chem. Soc.*, **1995**,117, 233-244.

12 R. D. McCullough, R. D. Lowe, M. Jayaraman, D. L. Anderson, *J. Org. Chem.*, **1993**, 58, 904-912.

13 W. B. Cui, J. Yuen, F. Wudl, *Macromolecules*, **2011**, 44, 7869-7873.

14 C. B. Nielsen, M. Turbiez, I. McCulloch, *Adv. Mater.*, **2013**, 25, 1859-1880.

15 R. S. Bhatta, D. S. Perry, M. Tsige, *J. Phys. Chem. A*, **2013**, 117, 12628-12634.

16 H. J. Son, W. Wang, T. Xu, Y. Y. Liang, Y. Wu, G. Li, L. P. Yu, *J. Am. Chem. Soc.*, **2011**, 133, 1885-1894.

17 W. A. Braunecker, S. D. Oosterhout, Z. R. Owczarczyk, R. E. Larsen, B. W. Larson, D. S. Ginley, O. V. Boltalina, S. H. Strauss, N. Kopidakis, D. C. Olson, *Macromolecules*, **2013**, 46, 3367-3375.

18 J. Kim, A-R. Han, J. Hong, G. Kim, J. Lee, T. J. Shin, J. H. Oh, C.Yang, *Chem. Mater.*, **2014**, 26, 4933-4942.

19 J. W. Rumer, S. Y. Dai, M. Levick, Y. Kim, M. B. Madec, R. S. Ashraf, Z. Huang, S. Rossbauer, B. Schroeder, L. Biniek, S. E. Watkins, T. D. Anthopoulos, R. A. J.

Janssen, J. R. Durrant, D. J. Procter, I. McCulloch, *J. Mater. Chem. C*, **2013**, 1, 2711-2716.

20 F. Silvestri, A. Marrocchi, *Int. J. Mol. Sci.*, **2010**, 11, 1471-1508.

21 H. J. Yun, H. H. Choi, S. K. Kwon, Y. H. Kim, K. Cho, *Chem. Mater.*, **2014**, 26, 3928-3937.

22 U. H. F. Bunz, *Chem. Rev.*, **2000**, 100, 1605-1644.

23 S. W. Thomas III, G. D. Joly, T. M. Swager, *Chem. Rev*., **2007**, 107, 1339-1386.

24 J. N. Wilson, U. H. F. Bunz, *J. Am. Chem. Soc.*, **2005**, 127, 4124 -4125.

25 H. Y. Wang, J. M. Lin, W. Huang, W. Wei, *Sensor Actuat. B Chem.*, **2010**, 150, 798-805.

26 C. A. Breen, J. R. Tischler, V. Bulovic, T. M. Swager, *Adv. Mater.*, **2005**, 17, 1981-1985.

27 I. B. Kim, H. Shin, A. J. Garcia, U. H. F. Bunz, *Bioconjugate Chem.*, **2007**, 18, 815-820.

28 J. Cremer, P. Bäuerle, M. M. Wienk, R. A. J. Janssen, *Chem. Mater*., **2006**, 18, 5832-5834.

29 F. Silvestri, A. Marrocchi, M. Seri, C. Kim, T. J. Marks, A. Facchetti, A. Taticchi, *J. Am. Chem. Soc.*, **2010**, 132, 6108-6123.

30 H. M. Qin, L. S. Li, F. Q. Guo, S. J. Su, J. B. Peng, Y. Cao, X. B. Peng, *Energy Environ. Sci.*, **2014**, 7, 1397-1401.

31 Y. Ie, S. Jinnai, M. Nitania, Y. Aso, *J. Mater. Chem. C*, **2013**, 1, 5373-5380.

32 H. Gao, Y. Q. Li, L. H. Wang, C. Y. Ji, Y. Wang, W. J. Tian, X. C. Yang, L. X. Yin,

Chem. Commun., **2014**, 50, 10251-10254.

33 S. L. Lu, M. J. Yang, J. Luo, Y. Cao, *Synth. Met.*, **2004**, 140, 199-202.

34 Z. L. Wu, B. H. Fan, Ai Y. Li, F. Xue, J. Y. Ouyang, *Org. Electron.*, **2011**, 12, 993-1002.

35 Y. H. Hou, Y. S. Chen, Q. Liu, M. Yang, X. J. Wan, S. G. Yin, A. Yu, *Macromolecules*, **2008**, 41, 3114-3119.

36 X. B. Huang, C. L. Zhu, S. M. Zhang, W. W. Li, Y. L. Guo, X. W. Zhan, Y. Q. Liu, Z. S. Bo, *Macromolecules*, **2008**, 41, 6895-6902.

37 W. Y. Wong, X. Z. Wang, Z. He, A. B. Djurišić, C. T. Yip, K. Y. Cheung, H. Wang, C. S. K. Mak, W. K. Chan, *Nat. Mater.*, **2007**, 6, 521-527.

38 F. R. Dai, H. M. Zhan, Q. Liu, Y. Y. Fu, J. H. Li, Q. W. Wang, Z. Y. Xie, L. X. Wang, F. Yan, W. Y. Wong, *Chem. Eur. J.*, **2012**, 18, 1502-1511.

39 T. A. Clem, D. F. J. Kavulak, E. J. Westling, J. M. J. Fréchet, *Chem. Mater.*, **2010**, 22, 1977-1987.

40 P. A. Troshin, O. A. Mukhacheva, Ö. Usluer, A. E. Goryachev, A. V. Akkuratov, D. K. Susarova, N. N. Dremova, S. Rathgeber, N. S. Sariciftci, V. F. Razumov, D. A. M. Egbe, *Adv. Energy Mater.*, **2012**, 3, 161-166.

41 M. Seri, A. Marrocchi, D. Bagnis, R. Ponce, A. Taticchi, T. J. Marks, A. Facchetti, *Adv. Mater.*, **2011**, 23, 3827-3831.

42 L. J. Huo, J. H. Hou, H.-Y. Chen, S. Q. Zhang, Y. Jiang, T. L. Chen, Y. Yang, *Macromolecules*, **2009**, 42, 6564-6571.

43 L. T. Dou, W.-H. Chang, J. Gao, C.-C. Chen, J. B. You, Y. Yang, *Adv. Mater.*,

2013, 25, 825-831.

44 L. T. Dou, J. Gao, E. Richard, J. B. You, C.-C. Chen, K. C. Cha, Y. J. He, G. Li, Y. Yang, *J. Am. Chem. Soc.*, **2012**, 134, 10071-10079.

45 Y. Wang, F. Yang, Y. Liu, R. X. Peng, S. J. Chen, Z. Y. Ge, *Macromolecules*, **2013**, 46, 1368-1375.

46 J. C. Bijleveld, M. Shahid, J. Gilot, M. M. Wienk, R. A. J. Janssen, *Adv. Funct. Mater.*, **2009**, 19, 3262-3270.

47 H. X. Zhou, L. Q. Yang, S. Stoneking, W. You, *ACS Appl. Mater. Interfaces*, **2010**, 2, 1377-1383.

48 J. W. Jung, J. W. Jo, F. Liu, T. P. Russell, W. H. Jo, *Chem. Commun.*, **2012**, 48, 6933-6935.

49 H. Y. Wang, B. Peng, W. Wei, *J. Polym. Sci. Poly. Phys.*, **2008**, 46, 1932-1938.

50 N. Zhou, X. Guo, R. P. Ortiz, S. Li, S. Zhang, R. P. Chang, A. Facchetti, T. J. Marks, *Adv. Mater.*, **2012**, 24, 2242-2248.

51 W. Yue, X. D. Huang, J. Y. Yuan, W. L. Ma, F. C. Krebs, D. H. Yu, *J. Mater. Chem. A*, **2013**, 1, 10116-10119.

52 Z. Li, Y. G. Zhang, S.-W. Tsang, X. M. Du, J. Y. Zhou, Y. Tao, J. F. Ding, J. *Phys. Chem. C*, **2011**, 115, 18002-18009.

53 D. M. De Leeuw, M. M. J. Simenon, A. R. Brown, R. E. F. Einerhand, *Synth. Met.*, **1997**, 87, 53-59.

54 C. Kanimozhi, P. Balraju, G. D. Sharma, S. Patil, *J. Phys. Chem. B*, **2010**, 114, 3095-3103.

55 Y. Zhu, R. D. Champion, S. A. Jenekhe, *Macromolecules*, **2006**, 39, 8712-8719.

56 Z. C. He, C. M. Zhong , X. Huang , W.-Y. Wong , H. B. Wu, L. W. Chen, S. J. Su, Y. Cao, *Adv. Mater.*, **2011**, 23, 4636-4643.

57 H. Y. Wang, F. Liu, L. Bu, J. Gao, C. Wang, W. Wei, T. P. Russell, *Adv. Mater.*, **2013**, 25, 6519-6525.

58 T. I. Ryu, Y. Yoon, J.-H. Kim, D.-H. Hwang, M. J. Ko, D.-K. Lee, J. Y. Kim, H. Kim, N.-G. Park, B. S. Kim, H. J. Son, *Macromolecules*, **2014**, 47, 6270-6280.

59 A. C. Mayer, M. F. Toney, S. R. Scully, J. Rivnay, C. J. Brabec, M. Scharber, M. Koppe, M. Heeney, I. McCulloch, M. D. McGehee, *Adv. Funct. Mater.*, **2009**, 19, 1173-1179.

60 Y. S. Liu, C.-C. Chen, Z. Hong, J. Gao, Y. Yang, H. Zhou, L. Dou, G. Li, Y. Yang, *Sci. Rep.*, **2013**, 3, 3356.

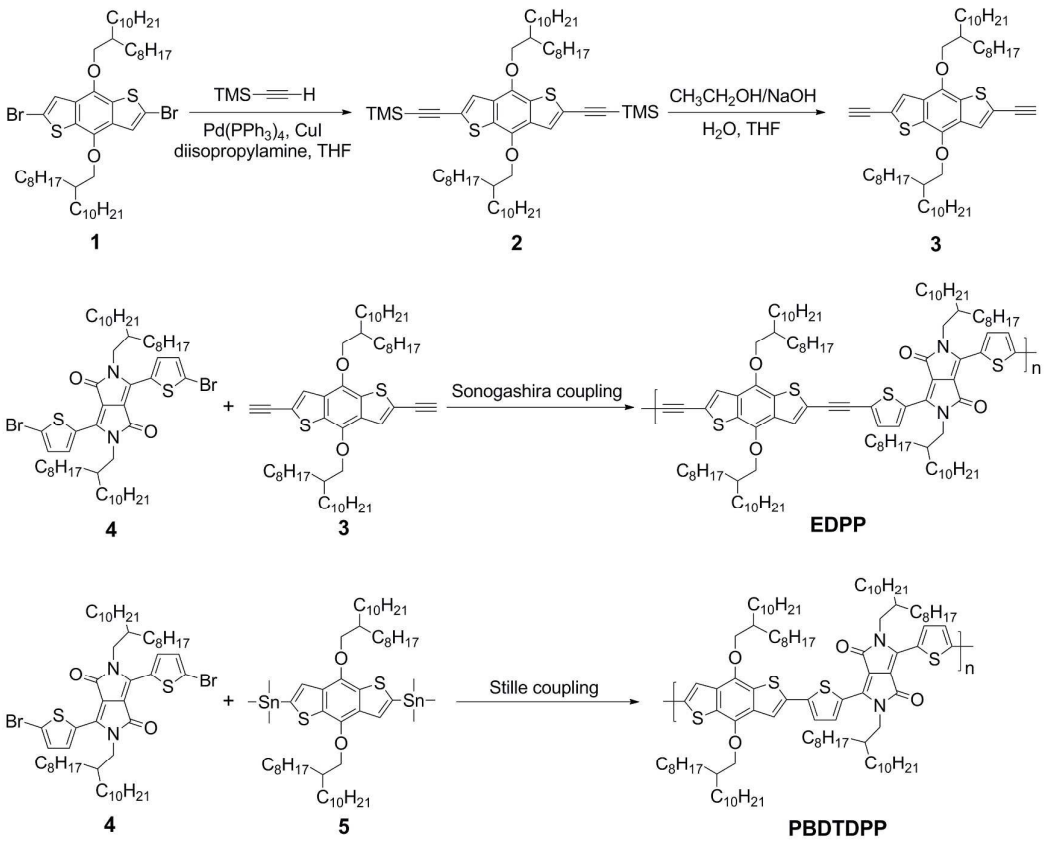

Scheme 1. Synthesis of **EDPP** and **PBDTDPP**.

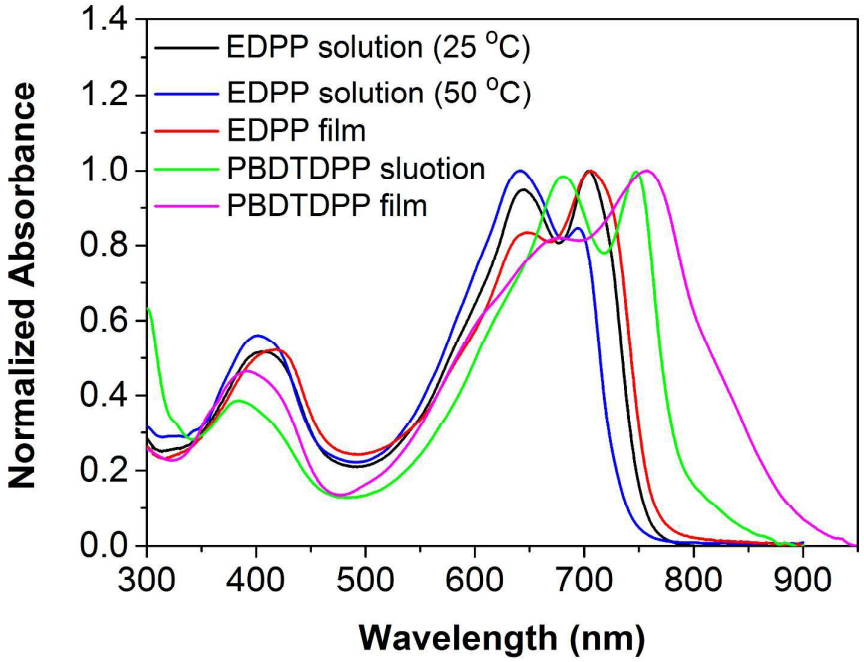

Fig. 1 UV-Vis absorption spectra of **PBDTDPP** and **EDPP** in chloroform solution and in thin films.

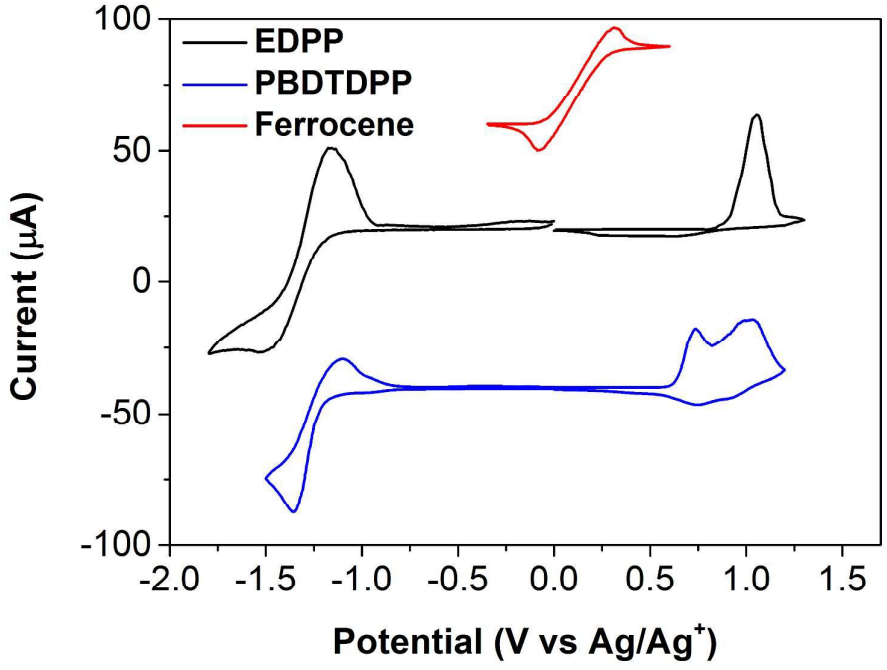

Fig. 2 Cyclic voltammograms of **PBDTDPP** and **EDPP** in CH_3CN/0.1 M n-Bu_4NPF_6.

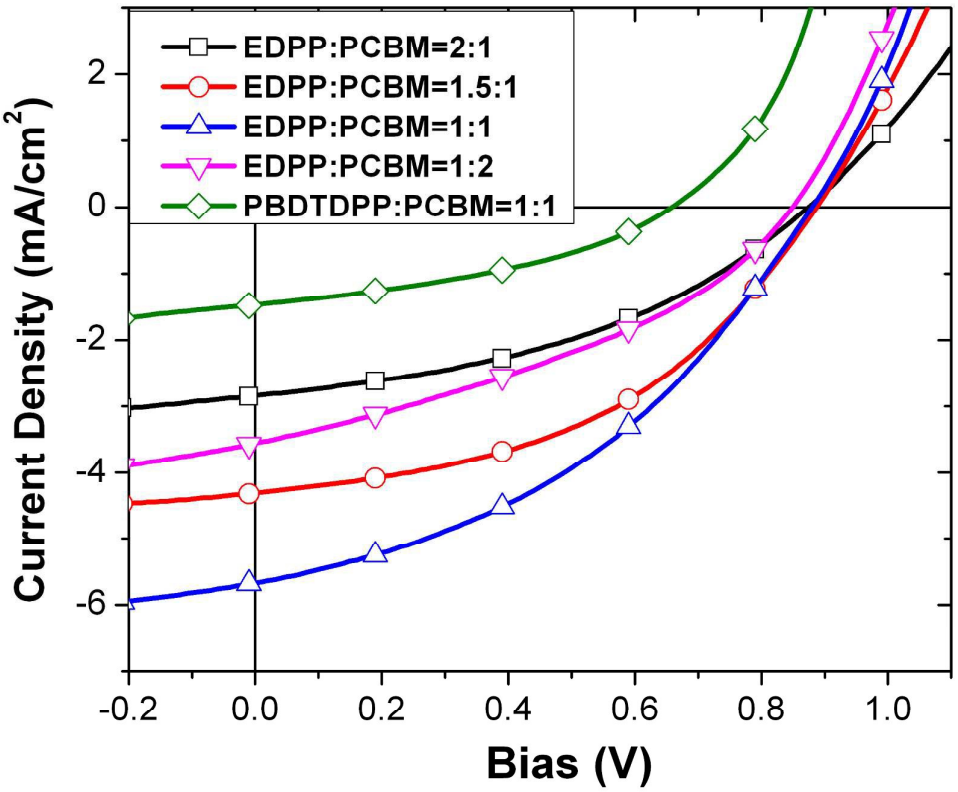

Fig. 3 Current density-voltage (*J*–*V*) curves with different weight ratios of polymer:$PC_{71}BM$ blends.

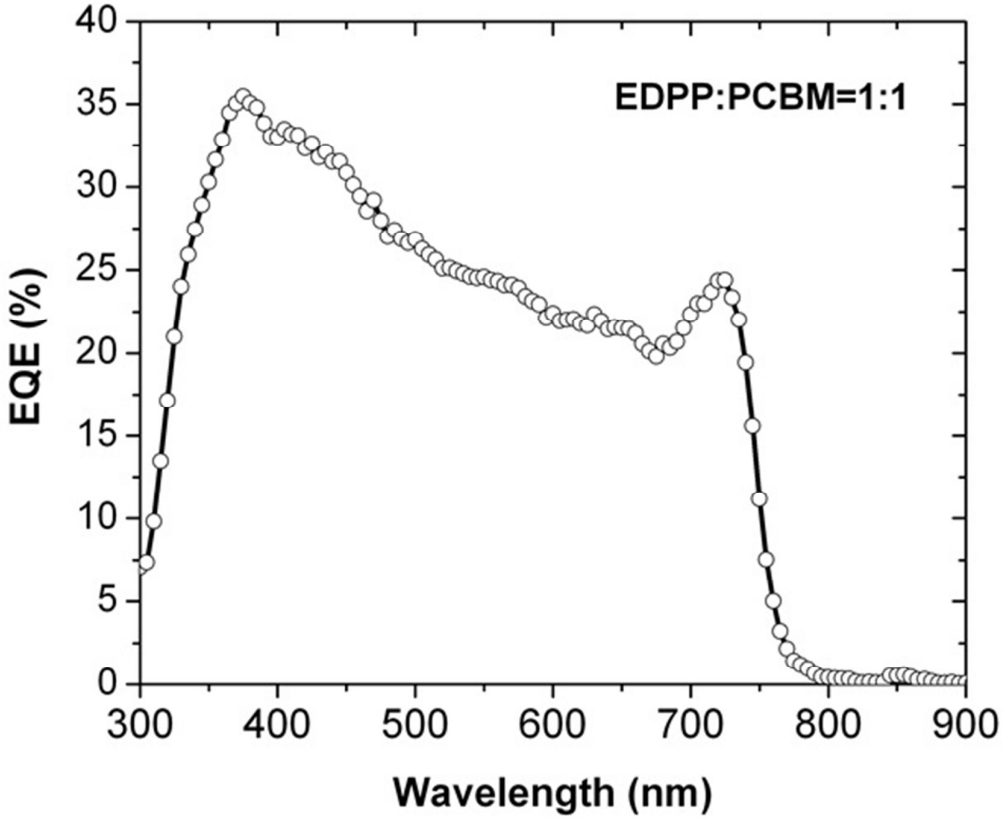

Fig. 4 EQE curve of **EDPP**:$PC_{71}BM$ device with weight ratio of 1:1.

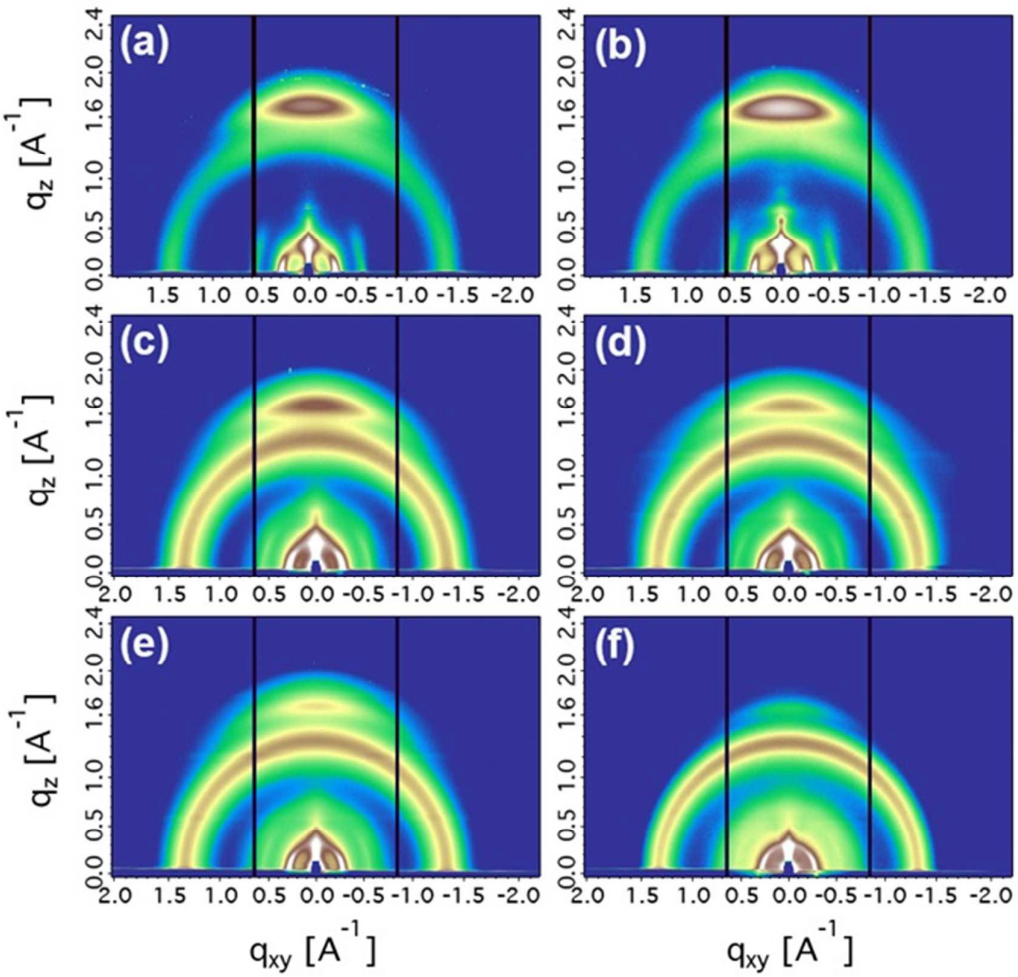

Fig. 5 GIWAXS profiles of (a) pure film, as spun; (b) pure film, annealed at 200 ^{o}C for 30 min; (c) **EDPP**:$PC_{71}BM$ = 2 : 1; (d) **EDPP**:$PC_{71}BM$ = 1.5 : 1; (e) **EDPP**:$PC_{71}BM$ = 1 : 1; (f) **EDPP**:$PC_{71}BM$ = 1 : 2.

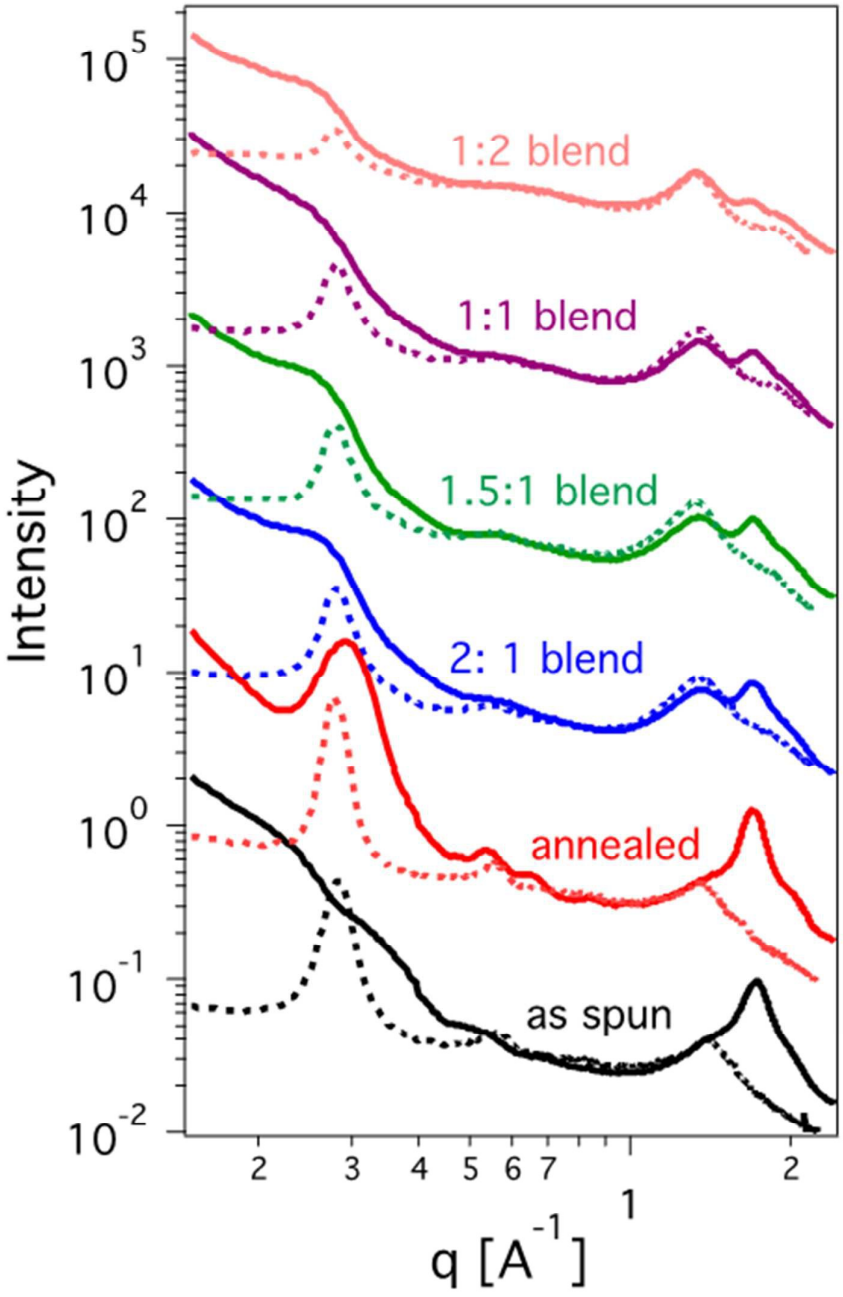

Fig. 6 Line-cut profiles of **EDPP** in pure film and blends. Solid line: out-of-plane cut, dashed line: in-plane cut.

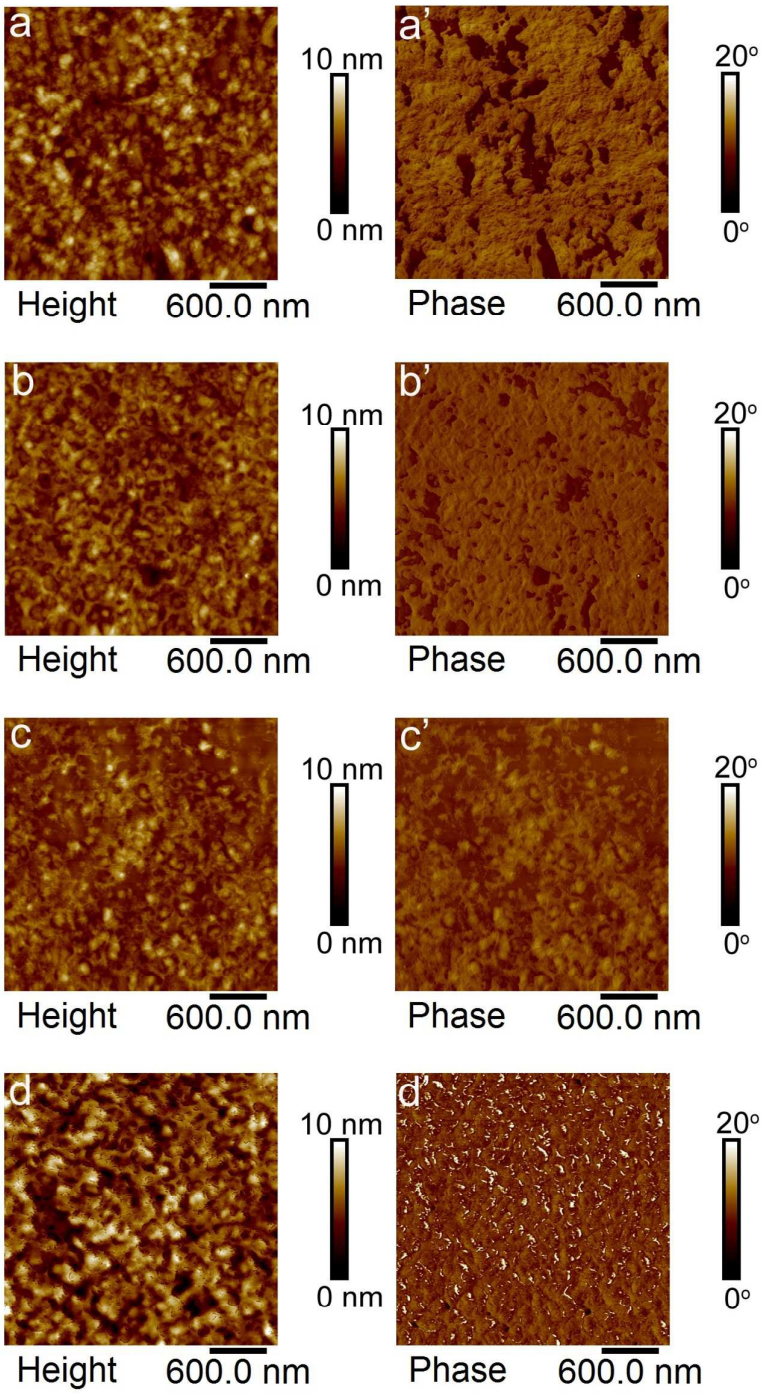

Fig. 7 Tapping-mode AFM height (left) and phase (right) images of the blend films. (a, a′) **EDPP**:$PC_{71}BM$ (2 : 1, w : w); (b, b′) **EDPP**:$PC_{71}BM$ (1.5 : 1, w : w); (c, c′) **EDPP**:$PC_{71}BM$ (1 : 1, w : w); (d, d′) **EDPP**:$PC_{71}BM$ (1 : 2, w : w).

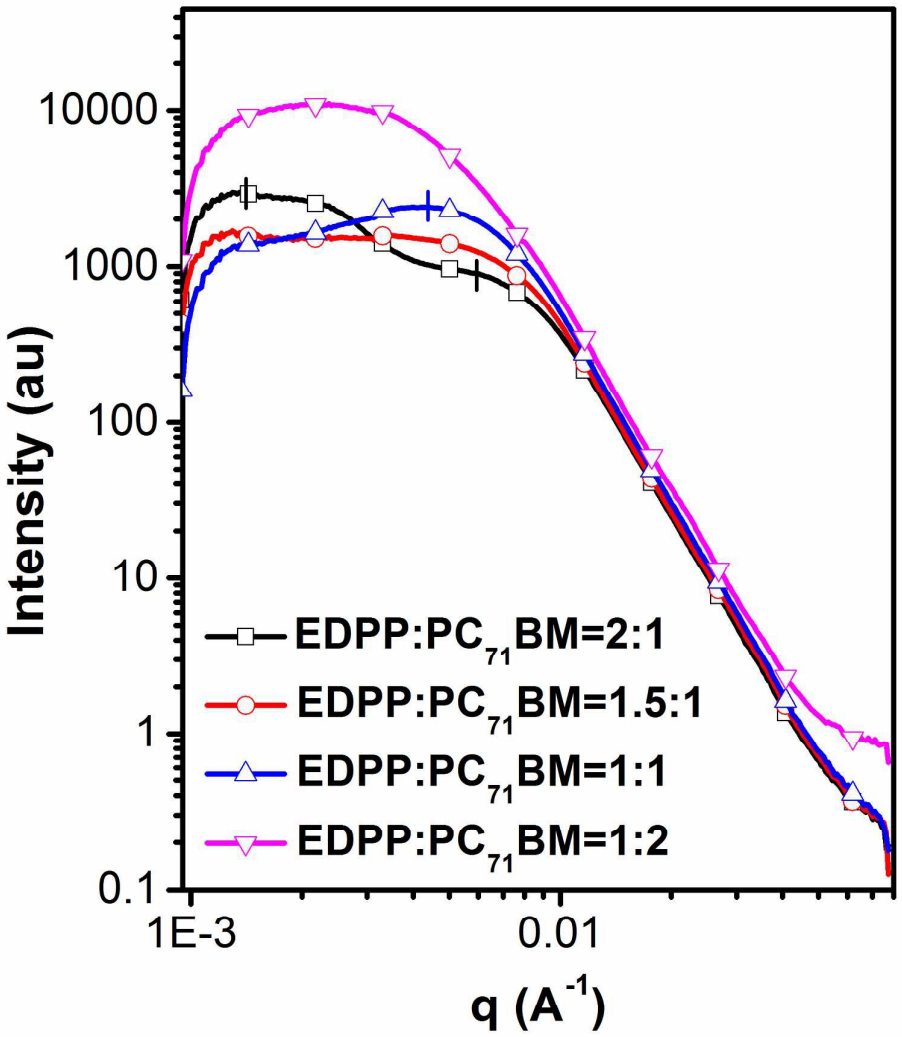

Fig. 8 RSoXS profiles of **EDPP**:$PC_{71}BM$ blends with different weight ratios.

Table 1. Molecular weight and optoelectronic properties of polymers.

Polymer	M_n [kg/mol]	PDI	λ_{max} sol [nm]	λ_{max} film [nm]	ε_{max} [a] [M^{-1} cm^{-1}]	$E_{g,opt}$ [b] [eV]	HOMO [c] [eV]	LUMO [c] [eV]
EDPP	46.3	2.55	645, 703	648, 707	6.19×10^4	1.55	-5.68	-3.63
PBDTDPP	10.2	2.11	681, 747	680, 758	5.22×10^4	1.31	-5.43	-3.61

[a] Extinction coefficient at λ_{max} in solution.

[b] Estimated from the absorption edge in thin films.Optical band gap =$1240/\lambda^{abs}_{onset}$ (eV).

[c]Estimated from the onset oxidation and reduction potential (vs Ag/Ag^+) plus 4.83.

Table 2. Photovoltaic data of the active layers with different compositions.

Blend ratios of **EDPP**:$PC_{71}BM$	V_{oc} (V)	J_{sc} (mA cm^{-2})	FF (%)	PCE (%)
2:1	0.87	2.84	40	1.0
1.5:1	0.88	4.31	45	1.71
1:1	0.88	5.67	39	1.98
1:2	0.84	3.55	37	1.10

Table 3. Data summary for GIWAXD.

Film	(1 0 0) [a]				(0 1 0)	
	q_{xy} ($Å^{-1}$)	$d_{(100)}$ (Å)	FWHM	CCL (nm)	q_z ($Å^{-1}$)	$d_{(010)}$ (Å)
EDPP (pure)	0.28	22.4	0.0325	19.3	1.72	3.65
EDPP (annealed)	0.28	22.4	0.0267	23.5	1.70	3.69
EDPP:$PC_{71}BM$ = 2:1	0.28	22.4	0.0338	18.6	1.70	3.69
EDPP:$PC_{71}BM$ = 1.5:1	0.28	22.4	0.0320	19.6	1.69	3.71
EDPP:$PC_{71}BM$ = 1:1	0.28	22.4	0.0339	18.5	1.70	3.69
EDPP:$PC_{71}BM$ = 1:2	0.28	22.4	0.0320	19.6	1.69	3.71

[a] (1 0 0) peak was determined from a Gaussian fit after background subtraction.

Graphical Abstract

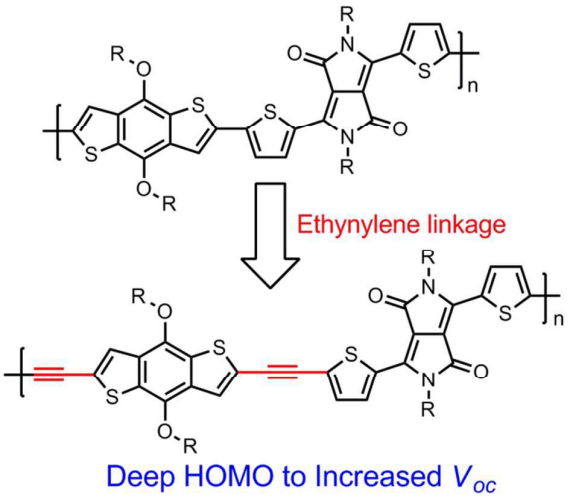

An ethynylene-linked benzo[1,2-*b*:4,5-*b*']dithiophene-*alt*-diketopyrrolopyrrole alternating copolymer was synthesized for increasing the V_{oc} of organic solar cells. And a high V_{oc} of 0.88 V was achieved due to the low-lying HOMO energy level.